Proposed Integration of Notch-Strain and Fatigue Crack-Growth Analyses

D. L. Ball*
General Dynamics/Fort Worth Division, Forth Worth, Texas

A model for the analysis of the growth of fatigue cracks in residual stress fields is developed by integrating notch-strain analysis techniques with linear-elastic fracture-mechanics-based crack-growth analysis techniques. The method by which elastic-plastic response stress gradients are estimated is presented along with a discussion of the use of those gradients in a fatigue crack-growth analysis. The modeling of crack-growth acceleration and retardation effects and their use after the stress response calculations are discussed. And in conclusion, the results of a newly developed computer program, which incorporates the combined techniques, are compared with crack-growth data from an in-service U.S. Air Force aircraft.

Nomenclature

A = fatigue crack-growth-rate acceleration factor
a = crack depth
C = fatigue crack-growth-rate equation coefficient
C_{pc} = plastic constraint factor
c = half-crack length
c_{eq} = equivalent half-crack length
d_{req} = crack depth and/or specimen thickness required to attain plane strain stress state
E = modulus of elasticity
K_I = mode I stress intensity factor
K_t = elastic stress concentration factor
m = Walker fatigue crack-growth-rate equation exponent
n = fatigue crack-growth-rate equation exponent
P = applied load
q = Chang fatigue crack-growth-rate acceleration index
R = stress ratio
r = hole radius
r_y = crack-tip plastic zone size
S_y = nominal or remote stress applied in the y direction
t = thickness
z = crack interaction zone size
β = stress intensity modification factor
ϵ_{yr} = estimated normal component in the y direction of the elastic-plastic response strain
μ = fatigue crack-growth-rate acceleration effectivity
ν = Poisson's ratio
σ_{ye} = normal component in the y direction of the elastic local (peak) stress
σ_{yr} = estimated normal component in the y direction of the elastic-plastic response stress

Introduction

THE modeling of fatigue crack growth in arbitrary, elastic-plastic stress fields is becoming an increasingly common, and in many cases, necessary part of damage tolerance analysis. The assumption of elastic, uniform stress is inappropriate for a wide variety of cases including those involving nonuniform applied stress, bending, structural overload, cold working of surfaces and fastener holes, welding, and structural and fastener interference. The usual approach taken in such problems is to determine a residual stress intensity factor based on some initial (static) residual stress field and then to superimpose that with the appropriate applied (cyclic) stress intensity factor. The methods discussed in Refs. 1-9 are typical. This "effective" stress intensity factor is then used to estimate the crack-growth rate, which in turn is integrated to find crack-growth life. As such, it fits neatly into existing linear-elastic fracture-mechanics (LEFM) based damage tolerance analysis methodology. However, none of these studies have addressed problems in which one or more of the spectrum load cycles are of such magnitude as to cause repeated yielding (and hence redefinition of residual stress fields) in the region of interest. This, on the other hand, is precisely what a notch-strain analysis[10] does, since it "tracks" material hysteresis behavior caused by plastic straining. These effects can be accounted for to a limited extent by using the one-dimensional analog of hysteresis loop tracking[11]: range pair or rain flow counting.[12] But both loop tracking and cycle counting techniques track the variation of stress at only a single point; they provide no information about the rest of the stress distribution in the area. Normally finite-element or boundary-element techniques are required for determination of complete response stress fields; but these are not practical for application in fatigue analyses involving potentially large numbers of cycles. And yet there exists a class of problems in which an LEFM-based fatigue crack-growth analysis could be successfully applied if modeling of plasticity due to structural configuration were introduced.

The following is a proposed integration of notch-strain analysis,[10] which is used extensively in fatigue crack-initiation studies, and cycle-by-cycle fatigue, crack-growth analysis[13] based on LEFM concepts. The model assumes localized yielding and attendant hysteresis effects to estimate response stress gradients on a given uncracked section on a cycle-by-cycle basis. Stress intensity factors are then calculated based on these gradients using Green's function techniques.

Discretization of Elastic Stress Distribution

The first step in the process involves the definition of one or more distributions of the component of elastic stress acting normal to a section which is coincident with the expected crack plane. In the discussion that follows, the section containing the crack will be taken to lie in the x-z plane, and the applied stress will act in the y direction. These stress distributions are the result of elastic stress analyses of the uncracked structure and as a result include geometric stress concentration effects. As shown in Fig. 1, each distribution is specified as a series of

Received Dec. 12, 1988; revision received Sept. 22, 1989. Copyright © 1989 by General Dynamics Corp., Fort Worth Division. Published by the American Institute of Aeronautics and Astronautics, Inc. with permission.

*Senior Engineer, Fatigue and Fracture Analysis.

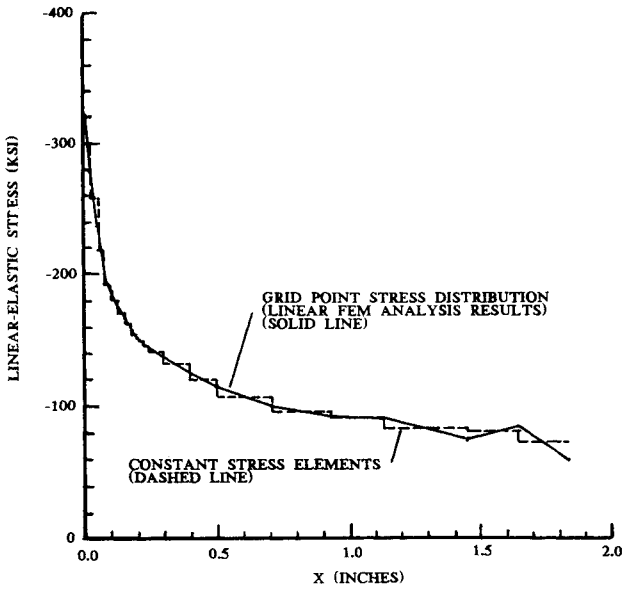

Fig. 1 Discretized stress distribution.

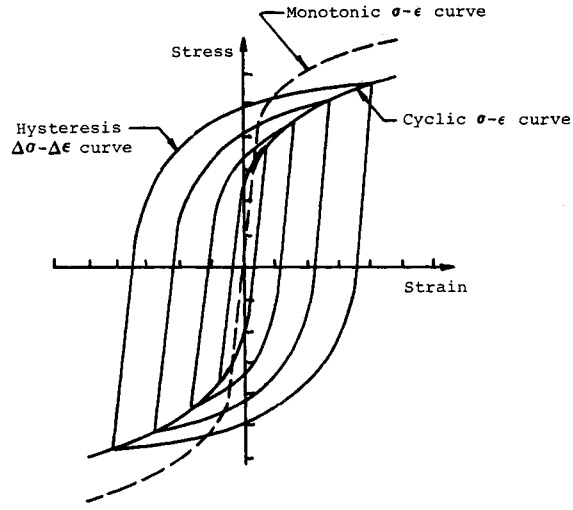

Fig. 2 Stable hysteresis loops from strain controlled test.

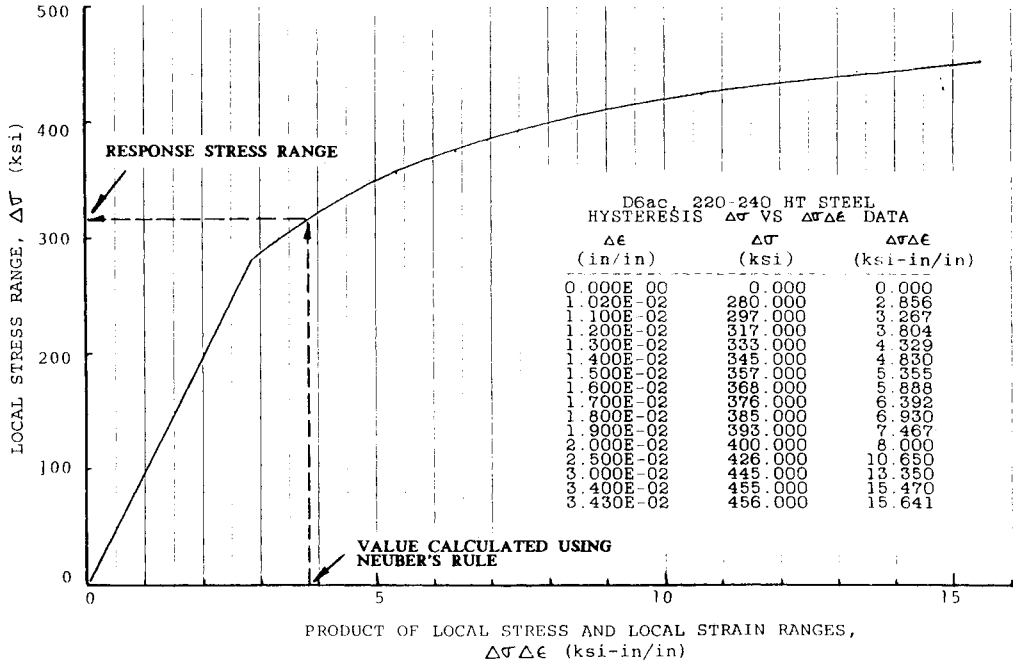

Fig. 3 Determination of local stress and strain ranges using Neuber's rule and material hysteresis stress vs stress-strain data.

n grid points and then approximated using $n-1$ constant stress elements. The stress value for each element is taken as the average of its endpoint values. Element widths are small in regions of high stress gradient and large in regions of relatively uniform stress. Since the analysis will require cycling between minimum and maximum stresses, provision is made for both negative and positive distributions in the event that structure/loading combinations yield distributions which are not of equal magnitude.

Calculation of Response Stresses

The stress response of each element of the distribution to the applied load is estimated using Neuber's rule[14] and notch-strain analysis techniques as described in Refs. 10 and 15. The application of this technique requires the definition of the cyclic and hysteresis stress vs strain curves for the material being studied. As shown in Fig. 2, the cyclic stress vs strain curve is given as the locus of the reversal points of stable hysteresis loops during strain controlled tests. The hysteresis stress-strain curve, represented by either the rising or falling portion of the hysteresis loop, is geometrically similar to the cyclic stress-strain curve and is generally found as in Ref. 16.

$$\sigma_{\text{hysteresis}} = 2\sigma_{\text{cyclic}} \tag{1}$$

To facilitate use with Neuber's rule, the hysteresis stress vs strain data is rewritten in terms of stress vs the product of stress and strain. See Fig. 3. The response stresses for each element are calculated on a point-to-point basis; that is, the applied stress is taken as the range between the current i and immediately preceding $i-1$ values. If the applied element stress range $\Delta\sigma_{ye}$ is less than the hysteresis proportional limit,

then the material behavior is considered to be linearly elastic and the response stress and strain are given by

$$\sigma_{yr_i} = \sigma_{ye_i} = \Delta\sigma_{ye} + \sigma_{yr_{i-1}} \tag{2}$$

$$\epsilon_{yr_i} = \Delta\sigma_{ye}/E + \epsilon_{yr_{i-1}} \tag{3}$$

where $\Delta\sigma_{ye}$ is the applied elastic element stress range specified by input stress gradients (Note: $\Delta\sigma_{ye} = K_t\Delta S$). Note that here and in the text that follows, i is the load point (reversal) counter, i.e., if a given cycle min is load point i, then the immediately following cycle max is load point $i + 1$. If the applied element stress range is greater than the hysteresis proportional limit, then Neuber's rule is used to calculate the true local stress and strain ranges:

$$\Delta\sigma_{yr}\Delta\epsilon_{yr} = \Delta\sigma_{ye}^2/E \tag{4}$$

Note again that the applied elastic stress range is assumed to include any stress concentration effects. With the stress-strain range product known, the response stress range $\Delta\sigma_{yr}$ and response strain range $\Delta\epsilon_{yr}$ may be determined using the material hysteresis stress-strain data as shown in Fig. 3. Finally, the response stress and strain are given by

$$\sigma_{yr_i} = \Delta\sigma_{yr} + \sigma_{yr_{i-1}} \tag{5}$$

$$\epsilon_{yr_i} = \Delta\epsilon_{yr} + \epsilon_{yr_{i-1}} \tag{6}$$

Since the origin of the hysteresis curve always corresponds with the stress reversal points and because the hysteresis curve is not modified with the application of stress cycles, "kinematic" material hardening is implied.

Local Stresses with Plastic Constraint

Assuming that the stress-strain response throughout the structure being analyzed is predominantly elastic, the stress state of the elements at a stress concentration will become increasingly triaxial as strains in the normal planar (x) and transverse (z) directions (due to the Poisson effect) are resisted by the surrounding elastic material.[17] The development of biaxial and triaxial stress states suggests the use of the equivalent stress from plasticity theory[18]

$$\sigma_{eq} = \frac{1}{\sqrt{2}}[(\sigma_1 - \sigma_2)^2 + (\sigma_2 - \sigma_3)^2 + (\sigma_3 - \sigma_1)^2]^{1/2}$$

$$= \frac{3}{\sqrt{2}}\tau_{\text{oct}} \tag{7}$$

where σ_1, σ_2, and σ_3 are the principal stresses, and τ_{oct} is the octahedral shear stress. This definition is convenient because, for uniaxial stress states, the equivalent stress reduces to the axial stress. In general, the model predicts the onset of yield when the equivalent stress equals the yield stress measured in a uniaxial tension test.

Because the equivalent stress is not dependent on the hydrostatic stress, the maximum principal stress at the notch root may exceed the uniaxial yield strength of the material by a considerable amount before the onset of yielding if a fully triaxial stress state develops. This phenomenon is known as "notch strengthening," and is exhibited by many ductile materials. Orowan[19] has demonstrated that the ratio of the maximum principal stress to the uniaxial yield strength of the material, often referred to as the "plastic constraint factor," may reach a maximum value of 2.57.

Since this apparent elevation of the yield stress can have a direct impact on the estimation of the magnitude and extent of nonlinear material response, the following simple approximation of the plastic constraint effect is used. The ratio of the x and z direction normal stress ranges to the y direction normal stress range is assumed constant:

$$\frac{\Delta\sigma_{xe}}{\Delta\sigma_{ye}} = \frac{\Delta\sigma_{ze}}{\Delta\sigma_{ye}} = \text{CSR} \tag{8}$$

where CSR is the constraint stress ratio. Using this approximation in Eq. (7), the equivalent stress range becomes

$$\Delta\sigma_{eq} = (1 - \text{CSR})\Delta\sigma_{ye} \tag{9}$$

The limiting values for CSR are found by noting that for plane stress $\Delta\sigma_{ze} = 0$ and therefore

$$\text{CSR}_{\min} = 0 \tag{10}$$

While for plane strain, we solve Eq. (9) for CSR and note that the maximum value for $\Delta\sigma_{ye}/\Delta\sigma_{eq}$ is 2.57, which yields

$$\text{CSR}_{\max} = 1 - 1/2.57 \tag{11}$$

The equivalent response stress and strain range are found by using the equivalent applied stress range in Neuber's rule

$$\Delta\sigma_{eq,r}\Delta\epsilon_{eq,r} = \Delta\sigma_{eq}^2/E \tag{12}$$

The estimated response stress range in the direction normal to the crack plane is assumed to be

$$\Delta\sigma_{yr} = \Delta\sigma_{eq,r}/(1 - CSR) \tag{13}$$

and the response stress is found using Eq. (5).

Load Redistribution Due to Plasticity

When the applied (elastic) stress range for a given element exceeds the hysteresis proportional limit, the response stress range will diverge from the elastic value due to material plasticity. The difference between the elastic and response stress values is an indicator of the reduction in load carrying capability of the element. In the current analysis, response stress gradients are approximated using the assumptions that the cross-section load and moment remain constant during local yielding. So the load "shed" by any one element must be picked up by the remaining elements.

Assuming that yielding occurs at element a, then the load which must be redistributed is given by

$$\Delta p_a = (\Delta\sigma_{yr_a} - \Delta\sigma_{ye_a})t dx_a \tag{14}$$

where t is the section thickness and dx_a is the element width. The load carried by the remaining elements of the cross section before redistribution is given by

$$P_{r,\text{old}} = \sum_{j=1}^{a-1} p_{j,\text{old}} + \sum_{j=a+1}^{n} p_{j,\text{old}} \tag{15}$$

and the load after redistribution is given by

$$P_{r,\text{new}} = \sum_{j=1}^{a-1} p_{j,\text{new}} + \sum_{j=a+1}^{n} p_{j,\text{new}} \tag{16}$$

where $p_{j,\text{new}}$ is calculated by assuming that the portion of Δp_a that is picked up by each element is given by

$$\Delta p_j = \Delta p_a \frac{p_{j,\text{old}}}{P_{r,\text{old}}} \tag{17}$$

The subscript j indicates that the calculations are for element j, and n is the total number of elements in the section. So the $p_{j,\text{new}}$ are found as

$$p_{j,\text{new}} = p_{j,\text{old}} + \Delta p_j \tag{18}$$

Since

$$p_{a,\text{new}} = p_{a,\text{old}} - \Delta p_a \tag{19}$$

and

$$\sum p_{j,\text{new}} = \sum p_{j,\text{old}} + \Delta p_a \tag{20}$$

the load carried by the cross section is unchanged. To conserve the moment carried by the cross section, the Δp_a that is subtracted from element a is added to an element b, which is equidistant from the cross-section centroid. And the Δp_j that are added to each element j are subtracted from the elements k again where elements j and k are equidistant from the cross-section centroid.

Once all of the Δp_j have been calculated, the new stress distribution may be found as follows

$$\sigma_{j,\text{new}} = \sigma_{j,\text{old}} + \Delta p_j/(t dx_j) \tag{21}$$

This process is repeated for element $a + 1$ and so on until all of the elements in the cross section have been checked and the load has been completely redistributed. Once all of the element stresses have been defined, the stresses at each grid point are taken as the average of the values of the elements sharing that grid point. And finally, the stress at any value of x is found by linear interpolation between grid point values.

This procedure is repeated for each reversal of the input fatigue load spectrum. For each cycle, the minimum response stress distribution is calculated, the subsequent maximum response distribution is calculated, and then the crack-tip stress-intensity factor is calculated for each based on these equations response distributions rather than the applied distributions.

Calculation of Stress Intensity Factors for Cracks Growing in Arbitrary Stress Fields

The stress intensity factors required for LEFM-based fatigue crack-growth analyses are typically found using both superposition and compounding techniques.[20] Total solutions for a given crack/geometry configuration subjected to a combination of loads may be found by superimposing the solutions for each load.

$$K_{I,\text{total}} = K_{I,1} + K_{I,2} + K_{I,3} \ldots \tag{22}$$

Whereas, those for a given load and crack-geometry configuration for which an exact solution is not available may be approximated using a factorial combination of the fundamental solution and one or more boundary/loading correction factors.

$$K_I = S\sqrt{\pi c}\,\beta_1\beta_2\beta_3 \ldots \tag{23}$$

where S is the nominal or reference stress; and β_1, β_2, β_3 is the boundary correction factor(s) as required by the geometry of the problem. The fundamental solution is that for a line (through-the-thickness, one-dimensional) crack in an infinite plate. In the current study, Green's functions are used to determine a "gradient" correction factor that may be compounded with known stress intensity factor solutions.

Green's Function Approach for Gradient Correction Factor

A common method for calculating the stress intensity factor for a crack in an arbitrary stress field is the Green's function approach described by Cartwright and Rooke.[21] This technique utilizes the preceding principle of superposition. For one-dimensional cracks in planar stress fields, the solution is developed in the following manner. Bueckner[22] demonstrated that the crack-tip stress-intensity factor for a stress-free crack in a stressed body is equivalent to that for a crack with an applied pressure distribution in an unstressed body when the applied pressure distribution is equivalent to the stress field that would exist if the stressed body were uncracked. This result is shown schematically in Fig. 4: the desired solution, case c, is found by superimposing two known solutions, cases a and b

$$K_{(c)} = K_{(b)} + K_{(a)} \tag{24}$$

Since the stress intensity factor for case b is zero, the total solution is given by the stress intensity factor for case a, which may be found by the method of Green's functions. An arbitrary pressure distribution on a line crack may be approximated as a series of point loads acting normal to the crack face.

$$p_j = \sigma(x)_j t dx_j \tag{25}$$

The Green's function for a point, crack opening force acting on a line crack in an infinite plate[23] is well known; see Fig. 5.

$$K_{I_j} = \frac{p_j}{t\sqrt{\pi c_{eq}}}\sqrt{\frac{c_{eq} + x}{c_{eq} - x}} \quad \text{(at crack tip A)} \tag{26}$$

The total stress-intensity factor is found by forming the sum

$$K_{I_{(a)}} = K_{I_{(c)}} = \sum_{j=1}^{m} \frac{p_j}{t\sqrt{\pi c_{eq}}}\sqrt{\frac{c_{eq} + x_j}{c_{eq} - x_j}} \tag{27}$$

where the crack face pressure distribution has been approximated using m point loads. In the limit, this summation be-

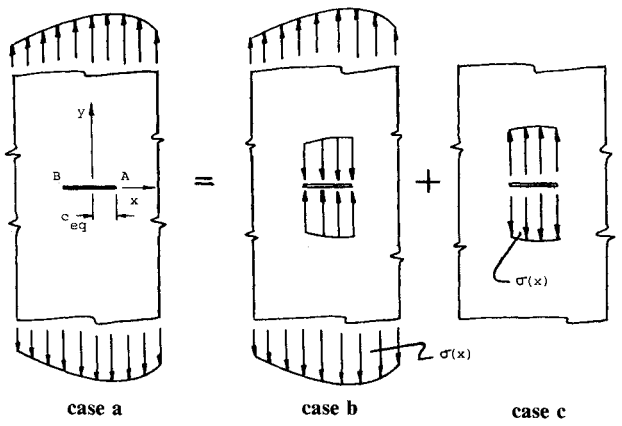

Fig. 4 Schematic illustration of equivalence between remote body loading and crack pressure loading.

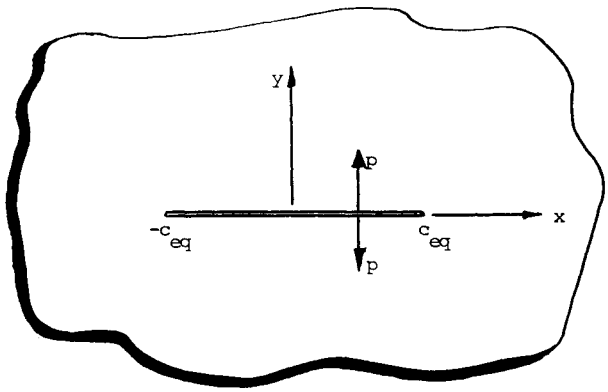

Fig. 5 Point load on a line crack in an infinite plate.

comes the integration of the Green's function over the crack length

$$K_I = \int_{-c_{eq}}^{c_{eq}} \frac{\sigma t}{t\sqrt{\pi c_{eq}}} \sqrt{\frac{c_{eq}+x}{c_{eq}-x}}\, dx \tag{28}$$

In order to isolate a stress intensity modification factor due to the gradient alone, the total solution must be written in terms of the fundamental form. To this end, the stress distribution is normalized with respect to some reference value, usually the gradient value at the site of crack initiation:

$$K_I = S\sqrt{\pi c_{eq}} \left[\frac{1}{\pi c_{eq}} \int_{-c_{eq}}^{c_{eq}} \frac{\sigma}{S} \sqrt{\frac{c_{eq}+x}{c_{eq}-x}}\, dx \right] \tag{29}$$

So the gradient correction factor becomes

$$\beta_g = \frac{1}{\pi c_{eq}} \int_{-c_{eq}}^{c_{eq}} \frac{\sigma}{S} \sqrt{\frac{c_{eq}+x}{c_{eq}-x}}\, dx \quad \text{(for crack tip A)} \tag{30}$$

The gradient correction factor for use with edge-cracked configurations may be derived in the same preceding manner using the point load solution for an edge-cracked, semi-infinite plate.[24] The result of that derivation is given as

$$\beta_g = \frac{2}{1.1215\pi c_{eq}} \left\{ \int_0^{c_{eq}} \frac{\sigma}{S} \frac{[1.3 - 0.3(x/c_{eq})^{5/4}]}{\sqrt{1-(x/c_{eq})^2}}\, dx \right\} \tag{31}$$

For completely arbitrary stress distributions, numerical integration is required for the evaluation of β_g. This is implemented by discretization of the stress distribution as just discussed and evaluation of the integral over each constant stress element

$$\beta_g = \frac{1}{\pi c_{eq}} \sum_{j=1}^{m} \left\{ \int_{a_j}^{b_j} \frac{\sigma_j}{S} \sqrt{\frac{c_{eq}+x}{c_{eq}-x}}\, dx \right] \tag{32}$$

for crack tip A of the infinite plate configuration, as in Fig. 5, and

$$\beta_g = \frac{2}{1.1215\ \pi c_{eq}} \sum_{j=1}^{m} \left\{ \int_{a_j}^{b_j} \frac{\sigma_j}{S} \frac{[1.3 - 0.3(x/c_{eq})^{5/4}]}{\sqrt{1-(x/c_{eq})^2}}\, dx \right\} \tag{33}$$

for the edge-crack (semi-infinite plate) configuration. The a_j and b_j are the x coordinates of the end points of the jth element, and the element m contains the crack tip. Because the path of integration includes the singularity at the crack tip, a 10-point Gauss-Legendre quadrature[25] is used to evaluate the integral over each element.

Since the gradient correction factors may in general be different for a positive gradient than they are for a negative gradient, total stress-intensity factor solutions are developed for both the maximum and minimum stresses. These solutions are calculated as a factorial combination of the fundamental solution, the gradient correction factor, and any other boundary correction factors that may be required by the geometry of the problem. In each case, care is taken that correction factors, which already include stress gradient effects, not be used when they duplicate the gradient factors just discussed. Discussion of this and other compounding techniques are provided in Refs. 26–28, and extensive compilations of total stress-intensity factor solutions are given in Refs. 24 and 28.

Load Interaction in Fatigue Crack-Growth Analysis

It is well recognized that nonlinear material behavior at the tip of a fatigue crack is probably the most significant contributor to load interaction effects (retardation and acceleration) in fatigue crack growth. The plasticity which is estimated in the preceding notch-strain analysis is based on the uncracked section only; it does not address the crack-tip plastic zone. No attempts to model the relationship and potential interaction between the residual stress field and the crack tip plastic zone were made during the current study.

Crack Tip Stress State and Plastic Zone Size Estimation

Using the arguments similar to those presented in the section "Local Stresses with Plastic Constraint" and treating the crack as a sharp notch, it has been demonstrated that for thin sections out-of-plane strains may develop freely producing a state of plane stress and the corresponding, relatively high values of fracture toughness. As the thickness increases, out-of-plane strains are increasingly constrained causing the development of a triaxial stress state and correspondingly reduced values of fracture toughness. Fracture toughness reaches a minimum when the normal in-plane and transverse strains at the crack tip are completely restrained and a state of plane strain is achieved (see Refs. 29–31). The dimension required to develop plane strain conditions is generally estimated as[32]

$$d_{\text{req}} = 2.5(K_{Ic}/F_{ty})^2 \tag{34}$$

This dimension may be used to estimate the state of stress at the crack tip during a fatigue crack-growth analysis in the following manner

$$C_{pc} = \min(c/d_{\text{req}}, t/d_{\text{req}}) \tag{35}$$

where we require that $0 < C_{pc} < 1$ and note that $C_{pc} = 0$ implies a state of plane stress and $C_{pc} = 1$ implies a state of plane strain.

Using the Irwin expressions for plane stress and plane strain plastic zone sizes,[32–34]

$$r_y = \frac{1}{2\pi} (K_{\max}/F_{ty})^2 \quad \text{plane stress} \tag{36}$$

$$r_y = \frac{1}{6\pi} (K_{\max}/F_{ty})^2 \quad \text{plane strain} \tag{37}$$

an expression for intermediate stress states may be written using C_{pc}

$$r_y = \frac{1}{(4C_{pc}+2)\pi} (K_{\max}/F_{ty})^2 \tag{38}$$

again, requiring that $0 < C_{pc} < 1$.

The estimated stress state may also be used to calculate the critical value of the stress intensity factor and hence the point of crack instability during a fatigue crack-growth analysis.

$$K_{\text{crit}} = K_c(1 - C_{pc}) + K_{Ic}C_{pc} \tag{39}$$

where K_{Ic} is the plane strain fracture toughness and K_c the fracture toughness at thickness of interest.

Yield Zone Interaction Model

The Willenborg[35,36] retardation model was selected for adaptation in the current analysis because it utilizes the concept of an "interaction" zone. According to Willenborg's original development, this would be the crack-tip plastic zone size due to the most recent tensile overload. In the current adaptation, this interaction zone may be the result of any plastic deformation, whether it be due to notch-strain effects or to the development of crack-tip plastic zone. Its size is taken as the larger of the effective crack length at the most recent overload or the distance to the elastic-plastic interface as determined by notch-strain analysis.

$$z = \max(z_{ol}, z_{nsa}) \tag{40}$$

where z is the interaction zone size; z_{ol} is the crack length at tensile overload plus size of crack-tip plastic zone due to

overload, $c_{ol} + r_{y,ol}$ (note that z_{ol} appears elsewhere in the literature as just the crack-tip plastic zone size at the tensile overload, $r_{y,ol}$); and z_{nsa} the distance between crack origin and elastic-plastic interface as determined by notch-strain analysis.

The original Willenborg model postulated that the interaction zone represented a region of "residual" stress and that this residual was equal to the difference between the applied (remote) stress and the stress required to terminate interaction, σ_{ap}. The σ_{ap} is the tensile stress required to generate an effective crack length (crack length plus crack-tip yield zone) equal to z_{ol}. This residual stress was then combined with the applied stress to determine the "effective" stress, i.e., that stress which is effective in growing the crack. The model was subsequently restated in stress intensity factor format by Gallagher[37,38] with the effective stress-intensity factors defined as

$$K_{\max,\text{eff}} = K_{\max} + K_{\text{res}} \tag{41}$$

$$K_{\min,\text{eff}} = K_{\min} + K_{\text{res}} \tag{42}$$

The residual stress-intensity factor K_{res} is defined as being proportional to the difference between the applied stress-intensity factor and the stress-intensity factor required to terminate interaction

$$K_{\text{res}} = \phi(K_{\max} - K_{ap}) \tag{43}$$

where ϕ is the constant of proportionality proposed by Gallagher.[38] The K_{ap} may be written in terms of the stress-intensity factor at the overload as

$$K_{ap} = K_{ol}[(z - c)/r_{y,ol}] \tag{44}$$

In the original model, z was always that caused by a tensile overload so that K_{res} was always negative thus reducing the applied stress intensity factor to some effective value. (Note that this model alters stress ratio but not stress range.) In the current model, those interaction zones defined by notch-strain analysis may represent either a tensile or a compressive residual stress field, and the residual stress intensity factor may be either negative (retarding) or positive (accelerating) accordingly.

Negative Stress Ratio Effects

The crack-growth-rate acceleration scheme due to Chang[13] was based on the proposition that the growth rate at a negative stress ratio is equal to some constant times the growth rate at a stress ratio of zero (for the same ΔK_{eff}).

$$da/dN_{(R<0)} = A\,da/dN_{(R=0)} \tag{45}$$

Chang purposed the following crack-growth-rate equation for negative stress ratios

$$da/dN_{(R<0)} = C[(1 + R^2)^q K_{\max}]^n \tag{46}$$

and recommended that the constant A be determined from constant amplitude test data. With A known, an acceleration index q could be determined as follows

$$C[(1 + R^2)^q K_{\max}]^n = AC[(1 - R_{\text{eff}})^{m-1}\Delta K]^n \tag{47}$$

$$q = \log A/[n \log(1 + R^2)] \tag{48}$$

where R is the local (as opposed to applied) stress ratio, where $R_{\text{eff}} = 0$ for $R < 0$, and where the expression is good for $R < 0$. Note that the Walker[39] crack-growth-rate equation was used for the $R = 0$ case.

For an assumed acceleration index q, the resulting acceleration factor may be determined as follows

$$A = (1 + R^2)^{nq} \tag{49}$$

The observed crack-growth acceleration that occurs at negative stress ratios may be attributed to the difference between the applied and local response stress levels and to the fact that only that portion of the stress-intensity factor range for which the crack is open is effective in advancing the crack. Assuming the following definitions: R = local (response) stress ratio including plastic zone size effects; R_{eff} = local stress ratio of tensile stresses, i.e., those which are effective in growing the crack, note that for $-\infty < R < 0$, $R_{\text{eff}} = 0$ and $0 < R < 1$, $R_{\text{eff}} = R$; ΔK = local (response) stress-intensity factor range; ΔK_{eff} = local tensile stress-intensity factor range, note that for $-\infty < R < 0$, $\Delta K_{\text{eff}} = K_{\max}$ and $0 < R < 1$, $\Delta K_{\text{eff}} = K$, consider the translation of da/dN vs ΔK data into da/dN_{eff} vs ΔK_{eff} data. For a given value of ΔK, applied at a negative stress ratio, the growth rate is da/dN. However, the effective stress-intensity factor range is

$$K_{\text{eff}} = (1 - R_{\text{eff}})K_{\max} = K_{\max} \text{ for } R < 0 \tag{50}$$

and the effective growth rate da/dN_{eff} is that determined at $K_{\max}$ on the $R = 0$ curve. This process is shown graphically in Fig. 6.

To some extent, the Walker equation alone will predict this effect, making the introduction of q and a separate rate equation unnecessary. A negative stress-ratio acceleration factor may be derived from the Walker equation as follows:

$$da/dN_{(R<0)} = A\,da/dN_{(R=0)} \tag{51}$$

$$C[(1 - R)^{m-1}\Delta K]^n = AC[(1 - R_{\text{eff}})^{m-1}\Delta K_{\text{eff}}]^n \tag{52}$$

$$A = \frac{[(1 - R)^{m-1}\Delta K]^n}{[(1 - R_{\text{eff}})^{m-1}\Delta K_{\text{eff}}]^n} \tag{53}$$

Using $\Delta K_{\text{eff}} = (1 - R_{\text{eff}})K_{\max}$ and $\Delta K = (1 - R)K_{\max}$:

$$A = \frac{[(1 - R)^m K_{\max}]^n}{[(1 - R_{\text{eff}})^m K_{\max}]^n} \tag{54}$$

$$A = [(1 - R)/(1 - R_{\text{eff}})]^{mn} \tag{55}$$

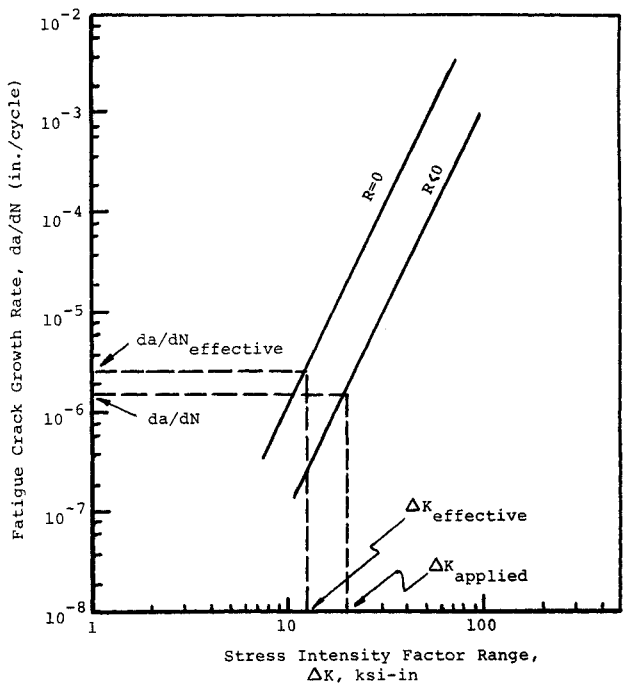

Fig. 6 Graphic estimation of negative stress ratio crack-growth-rate acceleration.

Since, by definition, $(1-R)/(1-R_{\text{eff}})>1$, the Walker equation will always provide negative stress-ratio acceleration when the product mn is greater than 1. However, since the Walker equation with coefficients based on positive stress-ratio da/dN data may not "fit" the corresponding crack growth-rate data in the negative stress-ratio regime, the following acceleration factor is proposed

$$A = [(1-R)/(1-R_{\text{eff}})]^{\mu mn} \tag{56}$$

where μ is the acceleration effectivity. The μ may be used to further "collapse" or "spread" the da/dN curves in the negative R regime when the data indicate that a value other than unity is required.

With the acceleration parameter defined in this manner, the same crack-growth-rate equation may be used in both the negative and positive stress ratio regimes

$$da/dN = AC[(1-R_{\text{eff}})^{m-1}\Delta K_{\text{eff}}]^n \tag{57}$$

when $R>0$, $R_{\text{eff}}=R$, and $A=1$. Therefore, the equation reduces to the Walker equation. When $R<0$, $R_{\text{eff}}=0$ and $A>1$ (again, assuming $\mu mn>1$). Note that $\mu=1$ does not indicate no acceleration, it indicates the acceleration provided by the Walker equation alone.

A corresponding acceleration factor for use with the Forman[40] crack-growth-rate equation may be developed as follows:

$$\frac{C\Delta K^n}{[(1-R)K_f-\Delta K]} = A\,\frac{C\Delta K_{\text{eff}}^n}{[(1-R_{\text{eff}})K_f-\Delta K_{\text{eff}}]} \tag{58}$$

$$A = \frac{[(1-R_{\text{eff}})K_f-\Delta K_{\text{eff}}]\Delta K^n}{[(1-R)K_f-\Delta K]\Delta K_{\text{eff}}^n} \tag{59}$$

$$A = [(1-R)/(1-R_{\text{eff}})]^{n-1} \tag{60}$$

Again, an acceleration effectivity parameter may be introduced yielding the following expression for A

$$A = [(1-R)/(1-R_{\text{eff}})]^{\mu(n-1)} \tag{61}$$

Application: F-111 Wing Pivot Fitting

In order to apply this technique, the preceding notch-strain methodology was programmed and integrated with an extensively modified version of the Air Force Detailed Fatigue Crack Growth Analysis Computer Program, CRKGRO.[41] The resulting program, CKGRO3, estimates uncracked elastic-plastic response stress gradients on a cycle-by-cycle basis. For each cycle the minimum and maximum stress intensity factors are calculated separately based on these response gradients and using the Green's function technique just discussed.

The development of this technique was brought about by the requirement for an analytical tool which was capable of predicting the growth of fatigue cracks in residual stress fields in general and in particular for the analysis of cracks in the wing pivot fitting of the F-111 aircraft. To insure flight safety, the F-111 aircraft is periodically subjected to a cold proof test in which the wings are statically loaded to both maximum and minimum limit loads. These high applied wing bending moments are sufficient to cause local yielding in areas of moderate to high stress concentration within the pivot fitting. See Fig. 7. As a result, any fatigue crack growth which may occur at such locations is dependent on both the residual stresses due to the cold proof test and the subsequent service load history.

The problem presented here is further complicated in that the control location is near the wing upper surface, which results in an applied fatigue spectrum that is compression dominated. The crack initiation site in this case is at the lower, inboard radius of fuel vent hole (FVH) no. 13. The general placement of the FVH within the center stiffener and the pertinent dimensions are shown in Fig. 8. The normal stresses acting on the section A-A (shown in Fig. 8) were determined from a previous, elastic, fine-grid finite-element analysis of the center stiffener in the area of FVH-13.[42] These results are tabulated for the +7.33 g limit load and the −2.4 g conditions in Table 1. (The +7.33 g distribution is also shown in Fig. 1.)

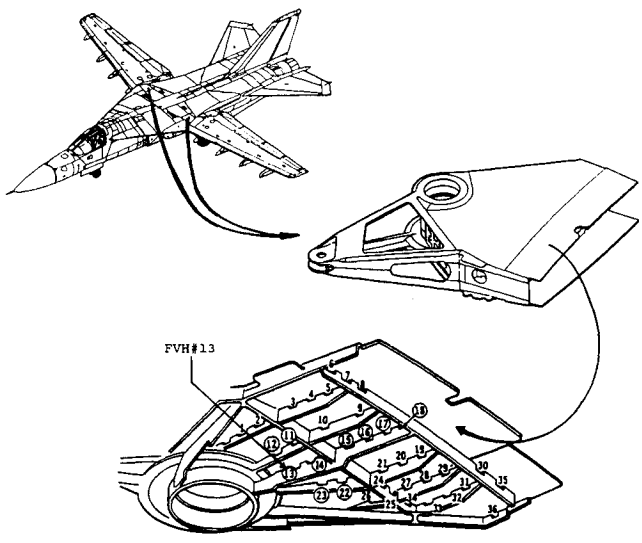

Fig. 7 Location of FVH-13 in wing pivot fitting of F-111 aircraft.

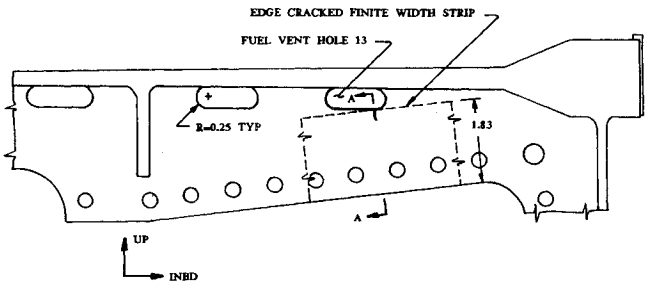

Fig. 8 F-111 wing pivot fitting, fuel vent hole 13.

Table 1 F-111 wing pivot fitting, FVH-13 elastic stress gradients

Grid no.	X coordinate, in.	Smin (CPT cond: +7.33 g), ksi	Smax (CPT cond: −2.40 g), ksi
1	0.000	−320.242	123.720
2	0.025	−279.163	109.920
3	0.050	−238.087	92.120
4	0.075	−197.010	74.319
5	0.100	−186.427	69.877
6	0.125	−175.843	65.434
7	0.150	−165.260	60.992
8	0.175	−158.992	58.418
9	0.200	−152.724	55.843
10	0.225	−146.986	53.484
11	0.250	−143.368	51.986
12	0.300	−136.130	48.989
13	0.400	−125.600	44.900
14	0.500	−115.070	40.810
15	0.710	−101.200	36.494
16	0.930	−93.150	33.761
17	1.120	−92.330	29.973
18	1.450	−75.700	26.106
19	1.650	−87.100	23.651
20	1.830	−57.250	21.724

Table 2 Six-point cold-proof test-load sequence

Step	Condition	Peak elastic stress, ksi
1	0.00	0.00
2	−2.40 *g*	123.72
3	+7.33 *g*	−320.24
4	−3.00 *g*	159.65
5	+7.33 *g*	−320.24
6	0.00	0.00

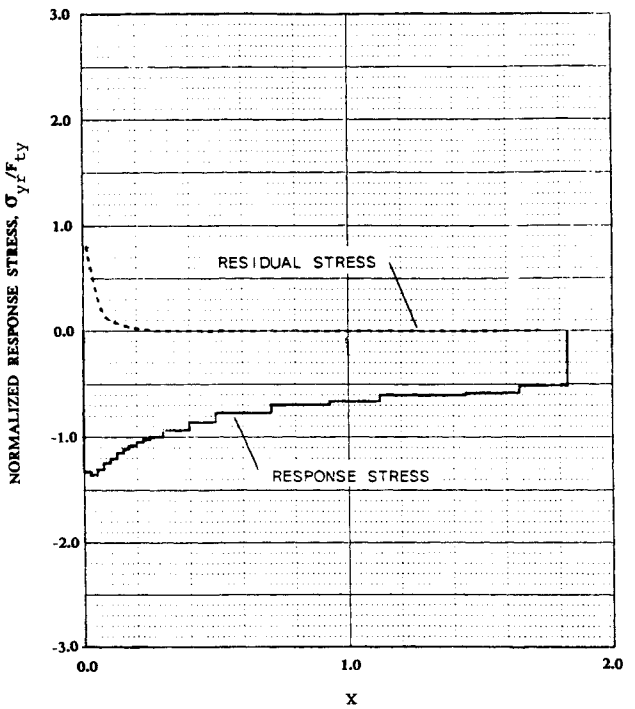

Fig. 9 Normalized response (solid line) and residual (dashed line) stresses through depth of stiffner for +7.33 *g* condition of F-111 cold proof test.

Both distributions are for a baseline FVH configuration, i.e., as shown in Fig. 8, and were used directly as the input minimum and maximum elastic stress gradients for CKGRO3. The response of the model (finite width strip) to the cold proof test load sequence (see Table 2) was analyzed using the elastic stress distributions shown in Table 1 and the hysteresis stress-strain data for the pivot fitting material 220–240 HT D6ac steel shown in Fig. 3.[43] The six-point sequence shown in Table 2 is an adaptation of actual test sequence with zero points placed before and after the CPT sequence; this forces the sequence into a min-max format as required by CKGRO3.

The variation of the total stress (response + constraint) and residual (zero applied strain) with depth into the stiffener is shown in Fig. 9 for the +7.33-*g* condition. Note that the analysis estimates both the shape and depth of the residual stress distribution. These results represent at least a qualitative, successful demonstration of the response stress estimation technique; actual validation will require verification testing and/or comparison with detailed stress analyses based on more accurate, continuum mechanical representation of the material behavior.

This approximation is useful because it may be repeated on a cyclic basis, thus modeling the creation and cyclic variation

Table 3 Forman crack-growth-rate equation parameters for D6ac steel, 220–240 HT

	Length direction	Depth direction
Plane strain fracture toughness	53.000	53.000
Plane stress fracture toughness	110.000	110.000
Region II		
Growth rate eq. const. *C*	1.091E-06	1.091E-06
Growth rate eq. exp. *N*	2.016	2.016
Growth rate eq. const. *KF*	110.000	110.000
Neg. stress ratio effectivity, *MU*	0.000	0.000
Region I		
Transition to lower curve	at 13.00 level 0.00E+00	
Growth rate eq. const. *C*	2.998E-09	2.998E-09
Growth rate eq. exp. *N*	4.317	4.317
Growth rate eq. const. *KF*	110.000	110.000
Neg. stress ratio effectivity, *MU*	0.000	0.000

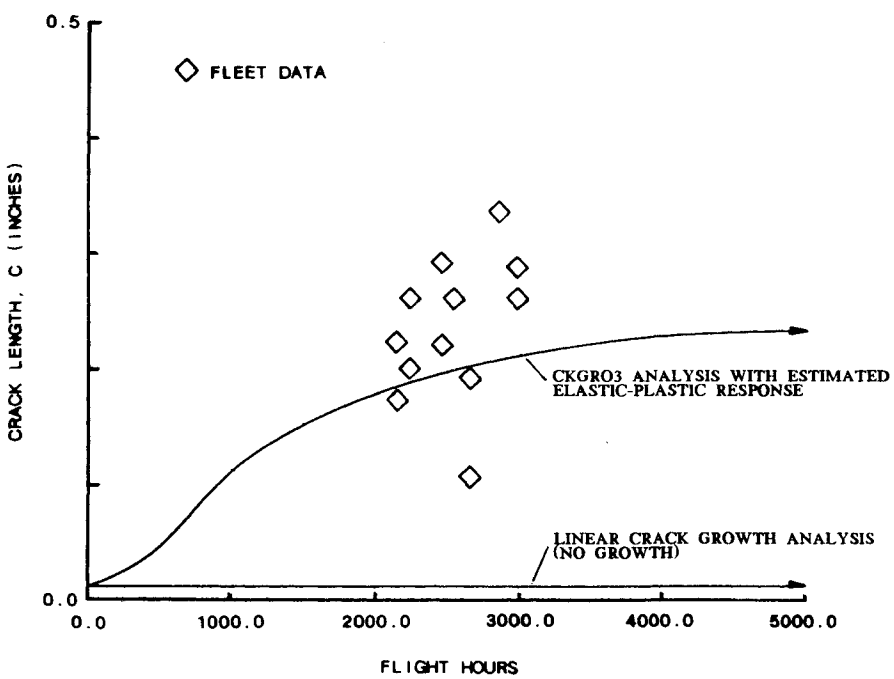

Fig. 10 Comparison of analytical crack growth lives with F-111A fleet cracking data.

of response stress and residual stress distributions on the uncracked section. With this information available, detailed fatigue crack-growth analyses are then conducted in the following manner.

1) Apply the precycle (CPT) load sequence as just described and calculate response stress gradients at each point using the stress-strain data shown in Fig. 3.

2) Calculate the response to the minimum and maximum applied spectrum stresses on a cycle-by-cycle (C×C) basis. Note that the hysteresis looping effect is modeled for each element in the cross section for each reversal in the spectrum.

3) Calculate the minimum and maximum stress-intensity factors based on stress gradients determined at each step using the Green's function technique.

4) Calculate crack growth rates and then crack length increments and integrate between the initial and final flaw sizes or until the critical value of stress intensity is reached. The Forman crack growth-rate equation parameters used for the wing pivot fitting analysis are shown in Table 3.[44] (The acceleration effectivity, $\mu = 0$, is based on comparison of the crack-growth-rate equation with $R = -0.5$ crack-growth-rate data.)

The results of two CKGRO3 fatigue crack-growth analyses, one with estimated elastic-plastic response calculation and the other without, are presented in Fig. 10. Comparison with the F-111 fleet cracking data shown in the same figure demonstrates the importance of modeling the creation of tensile residual stress fields. In each case, the spectrum crack growth analysis took place after the application of the CPT load sequence.

Conclusions

The use of notch-strain analysis techniques in lieu of finite-element or boundary-element techniques to model nonlinear material response of uncracked bodies to applied elastic stresses allows the approximation of local stress fields (including residual stresses) on a cyclic basis. The Green's function technique can then be employed to determine the stress intensity factors that result from the introduction of a crack. These techniques have been successfully integrated with a detailed fatigue crack-growth analysis computer program, and initial results indicate that for problems which involve moderate material plasticity and the development of residual stresses, this improved representation translates into improved LEFM-based fatigue crack-growth predictions.

Acknowledgment

This work was funded under Air Force Contract FO4606-84-D-0065 and was part of the F-111 Wing Pivot Fitting Fuel Venthole Damage Tolerance Analysis Update.

References

[1]Hall, L. R., Shah, R. C., and Engstrom, W. L., "Fracture and Fatigue Crack Growth Behavior of Surface Flaws and Flaws Originating at Fastener Holes, Vol. I," Air Force Flight Dynamics Laboratory, AFFDL-TR-74-47, May 1974.

[2]Shah, R. C., "On Through Cracks at Interference Fit Fasteners," *Transactions of the ASME, Journal of Pressure Vessel Technology*, Feb. 1977, pp. 75-82.

[3]Chang, J. B., "Prediction of Fatigue Crack Growth at Cold-worked Fastener Holes," *Journal of Aircraft*, Vol. 14, No. 9, 1977, pp. 903-908.

[4]Hsu, T. M., McGee, W. M., and Aberson, J. A., "Extended Study of Flaw Growth at Fastener Holes, Vol. I," Air Force Flight Dynamics Laboratory, AFFDL-TR-77-83, April 1978.

[5]Glinka, G., "Effect of Residual Stress on Fatigue Crack Growth in Steel Weldments Under Constant and Variable Amplitude Loads," *Fracture Mechanics*, Amercian Society for Testing and Materials, ASTM STP 677, 1979, pp. 198-214.

[6]Parker, A. P., "Stress Intensity Factors, Crack Profiles, and Fatigue Crack Growth Rates in Residual Stress Fields," *Residual Stress Effects in Fatigue*, American Society for Testing and Materials, ASTM STP 776, 1982, pp. 13-31.

[7]Nelson, D. V., "Effects of Residual Stress on Fatigue Crack Propagation," *Residual Stress Effects in Fatigue*, American Society for Testing and Materials, ASTM STP 776, 1982, pp. 172-194.

[8]Kim, C., Diesburg, D. E., and Ellis, G. T., "Effect of Residual Stress on Fatigue Fracture of Case-Hardened Steels—An Analytical Model," *Residual Stress Effects in Fatigue*, American Society for Testing and Materials, ASTM STP 776, 1982, pp. 224-234.

[9]Armen, H., Levy, A., and Eidinoff, H. L., "Elastic-Plastic Behvior of Coldworked Holes," *Journal of Aircraft*, Vol. 21, No. 3, 1984, pp. 193-201.

[10]Morrow, J., Martin, J. F., and Dowling, N. E., "Local Stress-Strain Approach to Cumulative Fatigue Damage Analysis," Dept. of Theoretical and Applied Mechanics, University of Illinois, T. & A.M. Rept. 379, 1974.

[11]Ball, D. L., and Neff, D. R., "Fatigue Load Spectrum Cycle Counting Methods," LTV Aerospace and Defense Co., Dallas, TX, SDM-1000, Nov. 1985.

[12]Dowling, N. E., "Fatigue Failure Predictions for Complicated Stress-Strain Histories," *Journal of Materials, JMLSA*, Vol. 7, No. 1, 1972, pp. 71-87.

[13]Chang, J. B., Hiyama, R. M., and Szamossi, M., "Improved Methods for Predicting Spectrum Loading Effects," USAF Wright Aeronautical Laboratories, AFWAL-TR-81-3092, Nov. 1981.

[14]Neuber, H., "Theory of Stress Concentration for Shear-Strained Prismatical Bodies with Arbitrary Nonlinear Stress-Strain Law," *Transactions of the ASME, Journal of Applied Mechanics*, Vol. 8, Dec. 1961, pp. 544-550.

[15]Wetzel, R. M., "Smooth Specimen Simulation of Fatigue Behavior of Notches," *Journal of Materials, JMSLA*, Vol. 3, No. 3, 1968, pp. 646-657.

[16]Fuchs, H. O., and Stephens, R. I., "Self Stresses and Notch Strain Analysis," *Metal Fatigue in Engineering*, Wiley, New York, 1980, pp. 125-146.

[17]Dieter, G. R., "Notch Effects," *Mechanical Metallurgy*, 2nd ed. McGraw-Hill, New York, 1976, pp. 280-284.

[18]Mendelson, A., "Criteria For Yielding," *Plasticity: Theory and Application*, Krieger, Malabar, FL, 1983, pp. 70-97.

[19]Orowan, E., *Transactions Inst. Shipbuild. Scot.*, Vol. 89, 1945, p. 165.

[20]Gallagher, J. P., Giessler, F. J., Berens, A. P., and Engle, R. M., Jr., "Introduction and Methodology Fundementals," *USAF Damage Tolerant Design Handbook*, Air Force Wright Aeronautical Laboratories, Wright-Patterson Air Force Base, OH, AFWAL-TR-82-3073, May 1984, pp. 1.6.1-1.8.25.

[21]Cartwright, D. J., and Rooke, D. P., "Green's Functions in Fracture Mechanics," *Fracture Mechanics—Current Status, Future Prospects*, edited by R. A. Smith, Pergammon, Toronto, 1979, pp. 91-123.

[22]Bueckner, H. F., "The Propagation of Cracks and Energy of Elastic Deformation," *Transactions of the American Society of Mechanical Engineers*, Vol. 80, Series E, 1958, pp. 1225-1229.

[23]Irwin, G. R., "Analysis of Stresses and Strains Near the End of a Crack Transversing a Plate," *Transactions of the ASME, Journal of Applied Mechanics*, Vol. 24, 1957, pp. 361-364.

[24]Tada, H., Paris, P. C., and Irwin, G. R., *The Stress Analysis of Cracks Handbook*, 2nd ed., Del Research Corp., Hellertown, PA, 1985.

[25]Press, W. H., Flannery, B. P., Teulkolsky, S. A., and Vetterling, W. T., "Integration of Functions," *Numerical Recipes*, Cambridge University Press, 1986, pp. 102-130.

[26]Newman, J. C., Jr., and Raju, I. S., "Stress Intensity Factor Equations for Cracks in Three-Dimensional Finite Bodies," NASA TM-83200, Aug. 1981.

[27]Ball, D. L., "The Development of Mode I, Linear-Elastic Stress Intensity Factor Solutions for Cracks in Mechanically Fastened Joints," *Engineering Fracture Mechanics*, Vol. 27, No. 6, 1987, pp. 653-681.

[28]Rooke, D. P., and Cartwright, D. J., *Compendium of Stress Intensity Factors*, Her Majesty's Stationery Office, London, 1976.

[29]Hertzberg, R. W., "Fracture Mode Transition: Plane Stress Versus Plane Strain," *Deformation and Fracture Mechanics of Engineering Materials*, Wiley, New York, 1976, pp. 279-282.

[30]Broek, D., "Plane Stress and Transitional Behavior," *Elementary Engineering Fracture Mechanics*, 4th ed., Nijhoff, Dordrecht, the Netherlands, 1986, pp. 194-227.

[31]Rolfe, S. T., and Barsom, J. M., "Effect of Temperature, Loading Rate and Plate Thickness on Fracture Toughness," *Fracture and Fatigue Control in Structures*, Prentice-Hall, Englewood Cliffs, NJ, 1977, pp. 92-139.

[32]Brown, W. F., and Srawley, J. E., *Plane Strain and Crack Toughness Testing of High Strength Metallic Materials,* ASTM STP 410, 1966.

[33]Irwin, G. R., "Fracture," *Handbuch der Physik,* Vol. VI, Springer, Berlin, 1958, p. 551.

[34]McClintock, F. A., and Irwin, G. R. "Plasticity Aspects of Fracture Mechanics," *Fracture Toughness Testing and its Applications,* ASTM STP 381, 1965, pp. 84–113.

[35]Willenborg, J. D., Engle, R. M., and Wood, H. A., "A Crack Growth Retardation Model Using an Effective Stress Concept," Air Force Flight Dynamic Laboratory, AFFDL-TM-FBR-71-1, Jan. 1971.

[36]Engle, R. M., and Rudd, J. L., "Analysis of Crack Propagation Under Variable Amplitude Loading Using the Willenborg Retardation Model," AIAA Paper 74-369, April 1974.

[37]Gallagher, J. P., "A Generalized Development of Yield-Zone Models," Air Force Flight Dynamics Laboratory, Wright-Patterson Air Force Base, OH, AFFDL-TM-74-28, 1974.

[38]Gallagher, J. P., and Hughes, T. F., "Influence of Yield Strength on Overload Affected Fatigue Crack Growth Behavior in 4340 Steel," Air Force Flight Dynamics Laboratory, AFFDL-TR-74-27, July 1974.

[39]Walker, K., "The Effect of Stress Ratio During Crack Propagation Fatigue for 2024-T3 and 7075-T6 Aluminum," *Effects of Environment and Complex Load History on Fatigue Life,* ASTM STP 462, 1970, pp. 1–14.

[40]Forman, R. G., Kearney, V. E., and Engle, R. M., "Numerical Analysis of Crack Propagation in Cyclic-Loaded Structures," *Transactions of the ASME, Journal of Basic Engineering,* Vol. 89, Series D, 1967, pp. 459–464.

[41]Chang, J. B., Szamossi, M., and Liu, K.-W., "A User's Manual for a Detailed Level Fatigue Crack Growth Analysis Computer Code, Vol. I—The CRKGRO Program," USAF Wright Aeronautical Laboratories, AFWAL-TR-81-3093, Nov. 1981 (b).

[42]Altstaeter, G. P., "Stress Analysis of the F-111 Wing Pivot Fitting Fuel Vent Hole 13," General Dynamics, Ft. Worth Div., FZS-12-531, March, 1987.

[43]Logan, B. J., and LaBar, B. G., "Final Engineering Report A8-112 Wing Pivot Fitting Failure Investigation Determination of Stiffener Runout Residual Stress," General Dynamics, Ft. Worth Div., FZS-12-454, April 1982.

[44]Hahn, W. J., and Nelson, M. E., "DADTA: F-111 A/E/D/F and FB-111A Final Analysis, Input Data and Analysis Methods," General Dynamics, Ft. Worth Div., FZS-12-494, Vol. 1, Sept. 1984.

ATTENTION JOURNAL AUTHORS:
SEND US YOUR MANUSCRIPT DISK

AIAA now has equipment that can convert virtually any disk (3½-, 5¼-, or 8-inch) directly to type, thus avoiding rekeyboarding and subsequent introduction of errors. The mathematics will be typeset in the traditional manner, but with your cooperation we can convert text.

You can help us in the following way. If your manuscript was prepared with a word-processing program, please *retain the disk* until the review process has been completed and final revisions have been incorporated in your paper. Then send the Associate Editor *all* of the following:

- Your final version of double-spaced hard copy.
- Original artwork.
- A *copy* of the revised disk (with software identified).

Retain the original disk.

If your revised paper is accepted for publication, the Associate Editor will send the entire package just described to the AIAA Editorial Department for copy editing and typesetting.

Please note that your paper may be typeset in the traditional manner if problems arise during the conversion. A problem may be caused, for instance, by using a "program within a program" (e.g., special mathematical enhancements to word-processing programs). That potential problem may be avoided if you specifically identify the enhancement and the word-processing program.

In any case you will, as always, receive galley proofs before publication. They will reflect all copy and style changes made by the Editorial Department.

If you have any questions or need further information on disk conversion, please telephone Richard Gaskin, AIAA Production Manager, at (202) 646-7496.